Journal Pre-proof

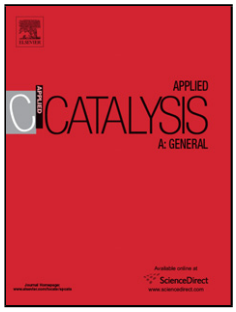

Re/AC catalysts for selective hydrogenation of dimethyl 1, 4-cyclohexanedicarboxylate to 1, 4-cyclohexanedimethanol: Essential roles of metal dispersion and chemical environment

Jingjie Luo (Conceptualization) (Investigation) (Writing - original draft), Enhui Qu (Data curation) (Investigation), Yixue Zhou (Validation), Yanan Dong (Formal analysis), Changhai Liang (Writing - review and editing) (Supervision) (Project administration) (Funding acquisition)

PII: S0926-860X(20)30262-3

DOI: https://doi.org/10.1016/j.apcata.2020.117669

Reference: APCATA 117669

To appear in: *Applied Catalysis A, General*

Received Date: 2 March 2020

Revised Date: 15 April 2020

Accepted Date: 27 May 2020

Please cite this article as: { doi: https://doi.org/

Re/AC catalysts for selective hydrogenation of dimethyl 1, 4-cyclohexanedicarboxylate to 1, 4-cyclohexanedimethanol: Essential roles of metal dispersion and chemical environment

Jingjie Luo, Enhui Qu, Yixue Zhou, Yanan Dong, Changhai Liang*

State Key Laboratory of Fine Chemicals and Laboratory of Advanced Materials & Catalytic Engineering (AMCE), School of Chemical Engineering, Dalian University of Technology, Panjin Campus, Panjin 124221, China.

* Corresponding author, E-mail: changhai@dlut.edu.cn (CH Liang)

Graphical Abstract

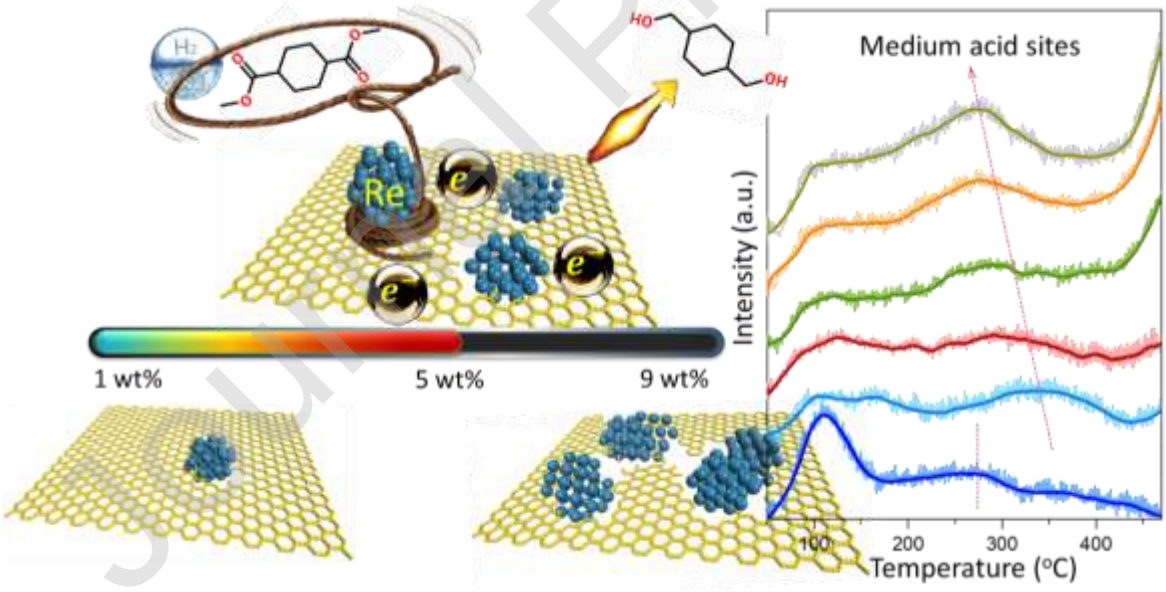

Highlights

- Pre-functionalized Re_x/AC are used for selective hydrogenation of diester to diol.
- Higher dispersion of exposed Re sites changes the textural and redox property.
- Electron is delivered from Re to C atoms leading to electron-deficient Re sites.
- New medium strong acid sites are generated due to fine ReO_x particles.
- Re_5/AC displays specific rate of 9.5×10^2 mmol $\cdot g_{Re}^{-1} \cdot h^{-1}$ at 220 °C in 10 MPa H_2.

Abstract

Rhenium, although viewed as one of the noble metals with lower-price, has been commonly used as doping element in the bimetallic catalysts due to its middlebrow to activate hydrogen. Its major role as catalyst is less frequently mentioned. In this work, rhenium has been decorated on the surface of activated carbon and used for the selective hydrogenation of dimethyl 1, 4-cyclohexanedicarboxylate (DMCD) to 1, 4-cyclohexanedimethanol (CHDM). Characterizations suggested that ReO_x particles were anchored occupying the surface oxygenated groups on pre-functionalized carbon. Rhenium decoration modified both the textural and chemical properties of the samples. Electrons were easily transferred from Re to the neighboring C atoms as a result of the formation of fine ReO_x particles. Medium strong acid sites were generated and rhenium species in the reduced states could be still maintained under appropriate rhenium dispersion. The moderate hydrogenation ability of rhenium catalyst partially restrained the excessive hydrogenation of CHDM to other by-products. Rational decoration of 5 wt% Re performed the better catalytic performance with complete conversion

of diester and 66% yield of diol. The specific rate reached $9.5 \times 10^2\ mmol_{DMCD} \cdot g_{Re}^{-1} \cdot h^{-1}$ at 220 °C under 10 MPa H_2.

Keywords: Rhenium catalyst, Selective hydrogenation, DMCD, CHDM, Activated carbon, Surface functionalization

1. Introduction

1, 4-cyclohexanedimethanol (CHDM) is a highly value-added organic compound extensively used in the polymer industry [1, 2]. It is noteworthy that CHDM is now preferred over ethylene glycol as a stepping-stone to produce polyester fibers [3, 4]. The most feasible catalytic route to date for producing CHDM is still a two-step process, via firstly the hydrogenation of dimethyl terephthalate (DMT) to dimethyl 1, 4-cyclohexanedicarboxylate (DMCD), and subsequently hydrogenated to CHDM in the temperature range of 200-300 °C under 3-15 MPa H_2 [5-7]. There are also successful one-pot synthesis of CHDM directly from DMT, unfortunately in the cost of lower conversion and turnover frequency, or the excessive loading of precious metals [7, 8]. No matter how on an industrial scale, the most feasible route to CHDM is the catalytic hydrogenation of DMCD by using Cu-Cr based catalysts. The toxicity of such additional Cr species leads to severe environmental problems, Cr-free catalysts with high efficiency are urgently to be designed.

In recent study, Hu et al. [9] have synthesized a series of Cu-Zn-Al catalysts used for the fixed-bed hydrogenation of DMCD to CHDM. The reduction process and the stably dispersed metallic Cu and Cu^+ species were confirmed to be a key point to activate the ester groups of

reactant. However, the reaction conditions were relative harsh under high pressure with huge H_2/DMCD ratio (406 mol/mol) and large dosage of catalyst (2.0-3.0 g). Other Ru or Pt based catalysts are also used as main catalysts for the production of CHDM, and bimetallic or even trimetallic catalysts have been designed for the reaction. The catalytic performance by using such multicomponent catalyst seems even mysterious to be understood, not to mention their unsatisfied activity. Besides, there is in fact not much work reported concerning the hydrogenation of ester groups of DMCD to CHDM. It is still of great importance to find new catalysts that are available to catalyze the hydrogenation of esters with well-established structure-performance relationship of catalysts.

Till now, precious metal based catalysts have displayed satisfied hydrogenation performance for many heterogeneous reaction [10, 11]. Different from other metals, Re precursor has the much lower price but inferior hydrogenolysis ability compared to other precious metals. It was reported that the additional Re species in precious metal based catalyst effectively adjust the dehydrogenation and C-O dissociation ability of active metal sites, remitting the excessive production of by-products [12-14]. Our previous work also suggested that using Re as dopant for the precious metal catalyst, fine distribution and smaller average sizes could be achieved [15, 16]. However until now, there is rarely report concerning the hydrogenation ability and the surface chemical environment of monometallic Re catalyst to understand the selective hydrogenation process of DMCD.

Under such circumstance, a series of ReO_x nanoparticles have been supported on activated carbon with different pre-treatments. The influence of Re decoration and pre-treatment on the

surface chemical composition, metal dispersion, and their rational performances on the selective hydrogenation ability have been studied in detail.

2. Experimental part

2.1 Materials

All chemicals and reagents were of analytical grade. The NH_4ReO_4 and activated carbon were purchased from Aladdin Chemical Co., Ltd. All the other chemical reagents such as the 37% H_2O_2 and concentrated HNO_3 employed in this study were obtained from Sinopharm chemical reagent Co. Ltd. Deionized (DI) water was used in the experiments.

2.2 Catalyst preparation

Activated carbon was preliminarily washed with boiled water to remove the residual ash content. It was previously reported that porous structure and the surface area, as well as the surface chemical environment might be modified in case of pre-treatments [17]. Herein, different pretreatments were used to modify the activated carbon: i) activated carbon was thermally treated under pure H_2 at 800 ^oC for 10 h, and denoted as AC-H; activated carbon was treated by ii) 37% H_2O_2 aqueous solution for 5 h or iii) concentrated HNO_3 solution for 5 h, denoted as AC-HO and AC-N, respectively; vi) thermally treated by H_2 and subsequently by concentrated HNO_3 solution for 5 h, denoted simply as AC. Wash and filter of samples were necessary until the pH value of solution reaches 7.0.

Re based catalysts have been prepared by incipient wetness impregnation. Certain amount of NH_4ReO_4 as precursor was dissolved in distilled water. 1g activated carbon was added into

the aqueous solution of Re precursor with stirring and sonicated for 30 min. The mixture was aged for 16 h and dried directly overnight in an oven under 60 ^{o}C. The as-obtained dry powder is label as Re_x/AC-y (x=1, 3, 5, 7, 9; y suggests the type of pretreatment).

2.3 Characterization

Transmission electron microscopy (TEM) was performed on a FEI Tecnai F30 electron microscope at an acceleration voltage of 120 kV. Before each observation, the catalyst was dissolved in solvent and treated in sonication for 10 min. Several drops of the supernatant liquid were added and evaporated on the copper grid. BET surface area and the pore structure of the catalysts were investigated using N_2 physical adsorption/desorption at -196 °C on an automatic volumetric sorption analyzer (Quantachrome, Autosorb-iQ-C). The specific surface area was calculated by the BET equation and the pore size was derived from the desorption branch of the isotherms by BJH method. Temperature-programmed reactions were operated on a Quantachrome ChemStar3000 equipment. H_2-temperature-programmed reduction (H_2-TPR) was tested using 100 mg sample. The sample was purged in Argon for 2 h at room temperature. After the gas atmosphere was changed to the mixture of 10% hydrogen in argon, the reduction data was recorded in the range of 50-800 ^{o}C. During the ammonia temperature-programmed desorption (NH_3-TPD), reduced catalyst (100 mg) was pre-treated by NH_3/He gas mixture at 50 ^{o}C for 1 h. After purged with He, the desorption was carried out and recorded from 50 to 700 ^{o}C. X-ray diffraction (XRD) measurements were carried out within 10^{o} -80^{o} on the Shimadzu XRD-7000S diffractometer with a Cu Kαradiation at 40 kV and 30 mA. X-ray photoelectron spectroscopy (XPS) measurements were performed on an ESCALAB™

250Xi (Thermo Fisher, USA) with the monochromatic Al Kα (1486.6 eV) X-ray source. CO chemisorption was carried out using a Micrometer Autochem 2910 instrument. The Raman spectra was recorded using a 532 nm laser source by Renishaw's in Via Confocal Raman Microscope. The surface defect density was evaluated according to the equation proposed by Cançado et al. [18].

$$\boldsymbol{n_D(cm^{-2}) = (7.3 \pm 2.2) \times 10^9 E_L^4 \left(\frac{I_D}{I_G}\right)}$$

where I_D/I_G is the ratio of peak intensity by height in Raman spectra locating around 1340 cm^{-1} and 1570 cm^{-1}. E_L is the excitation energy around 2.41 eV for single layer and few layer graphene [19].

Before each characterization, the catalyst was reduced under H_2/Ar atmosphere at 460 °C for 3 h, to ensure their identical condition as those before the reaction test, except the H_2-TPR.

2.4 Catalyst Evaluation

Liquid-phase hydrogenation was performed in 50 mL autoclave with electric temperature controller. Certain amount of reactant dimethyl 1, 4-cyclohexanedicarboxylate (DMCD) was dissolved in isopropanol with 125 mg catalyst pre-reduced by H_2/Ar under 460 °C for 3 h. The reactor was purged with hydrogen for three times to remove residual air and the aimed reaction pressure was set. The reactor was heated subsequently to the desired temperature under constant stirring. After reaction, the reactor was cooled down to room temperature. The liquid samples were analyzed by gas chromatograph (GC-7890F, FID, FFAP column 30 m×0.32 mm ×0.5 mm) using the P-xylene as internal standard.

The conversion of DMCD (x_{DMCD}), selectivity (S_i) and the relative yield (Yi) of different products were calculated by the following equations [20]:

$$\text{Conversion}(x_{DMCD}) = \frac{n_0 - n_t}{n_0} \times 100\%$$

$$\text{Selectivity}(S_i) = \frac{n_i}{\sum n_i} \times 100\%$$

$$\text{Yield}(Yi) = x_{DMCD} \times S_i \times 100\%$$

Where n_0 represents the initial number of moles of DMCD and n_t represents the number of moles of DMCD at time t. n_i represents the molar quantity of product i.

The specific reaction rate to convert one mmol of DMCD, based on per gram of surface exposed active metal per hour, was evaluated by the following equation:

$$\text{R} = \frac{n_{conv.} \cdot 10^{-3}}{m_{Re} \cdot D_{disp.} \cdot t} mmol \cdot g_{Re}^{-1} \cdot h^{-1}$$

Where $n_{conv.}$ is the number of moles of converted DMCD, in mmol; m_{Re} is the mass of Re species in use, in gram; $D_{disp.}$ is the surface dispersion of active metal sites tested by CO chemisorption; and t is the reaction time, in hour.

3. Results and discussion

3.1 Chemical composition and texture properties of Re$_x$/AC

The morphology of the reduced sample is revealed by TEM images as shown in Figure 1A. The black spots in each sample should be Re-containing particles due to the big atomic number of Re compared to C. Only very few amount of particles can be observed in the Re_1/AC sample, due to the lower Re content. The average particle sizes of Re_3/AC, Re_5/AC, and Re_9/AC samples are calculated to be 2.1, 3.7, and 5.3 nm, respectively, based on the

statistical results of more than 200 particles. Re species are easily dispersed on the surface of activated carbon without obvious sintering of huge particles. As the amount of rhenium increases, both small and bigger particles appear mainly caused by the slight accumulation of Re element, especially in the Re_9/AC sample.

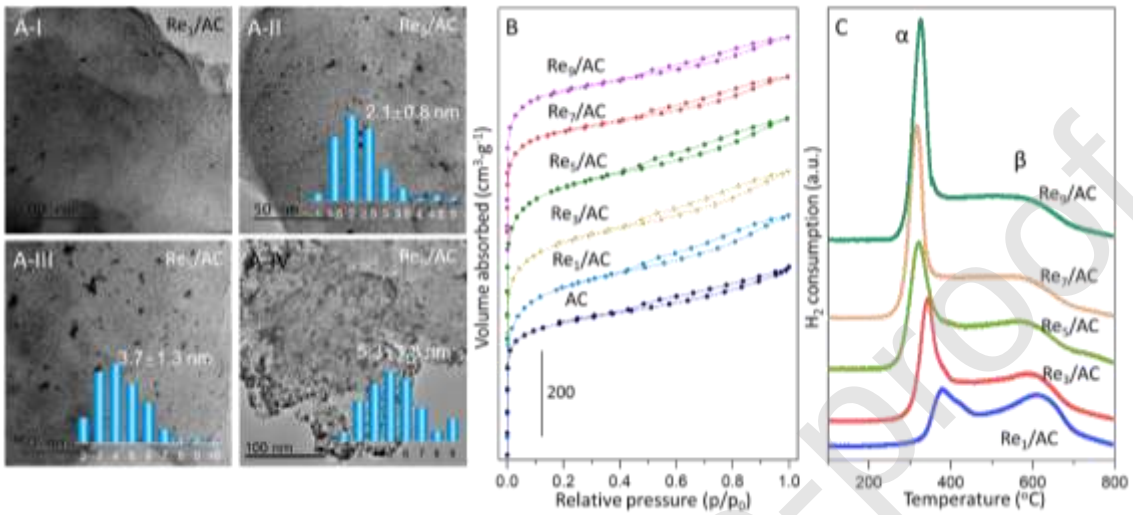

Figure 1. TEM images (A), N_2 adsorption/desorption isotherms (B) and H_2-TPR spectra (C) of the reduced Re_x/AC samples.

The influence of Re species on the structure of activated carbon has been detected by the N_2 adsorption/desorption isotherms (Figure 1B). The BET surface areas and the average pore sizes of different samples are listed in Table 1. The tested samples display the typical isotherms of type I (<0.02) with microspore filling and type IV by capillary condensation at high pressure, suggesting the co-presence of micro- and meso-pores [21, 22]. The H4 hysteresis loop exists at relative pressure (P/P_0) of 0.5-1.0 [23], mainly due to the inter-particle textural pores in the carbon materials. The surface areas of the Re_x/AC samples change from 541 to 370 m^2/g as the Re content increases to 7-9 wt%. The average pore sizes also slightly decrease from 4.6 nm to 4.2 nm. In fact, the initial surface area of activated carbon is 486 m^2/g and the average pore size is 4.6 nm. The decoration of Re causes the incrementing of the surface area without

great change on the pore size, especially if the Re content was lower (e.g. Re_1/AC and Re_3/AC). It is inferred that the additional doping and calcination processes in the Re_x/AC samples may result in the rough surface of carbon, which contributes to the larger surface area in turn. However, as the Re content raises, the metal particles are accumulated on the surface of carbon and may partially occupy the pores accounting for the loss of both the surface area and pore sizes.

Table 1 Textural property and surface information of different Re based catalysts.

Sample	BET		Defect density ($\times 10^{11}$ cm^{-2})	H_2 uptake[a] (μmol/kg)	Metallic surface area (m^2/g)[b]	Metal disper.[b]	Specific rate ($\times 10^2$ $mmol_{DMCD}/g_{Re}/s$)[c]
	Surface area (m^2/g)	Pore size (nm)					
Re_1/AC	541	4.6	5.15	17.3	21.1	10.0%	11.9
Re_3/AC	531	4.6	4.88	25.2	28.3	13.5%	7.0
Re_5/AC	554	4.4	4.90	31.4	21.8	6.2%	7.7
Re_7/AC	450	4.3	4.73	34.2	30.5	14.5%	2.3
Re_9/AC	370	4.2	4.65	40.2	40.1	19.1%	1.3
Re_5/AC-HO	642	3.3	4.85	-	11.4	6.4%	5.5
Re_5/AC-N	588	3.8	4.90	-	22.0	10.5%	4.0
Re_5/AC-H	612	4.7	4.83	-	5.2	2.4%	2.5

[a] H_2 consumption of α peak in H_2-TPR evaluated after peak deconvolution.

[b] Metallic surface area and metal dispersion evaluated by CO chemisorption.

[c] Specific rates of Re_x/AC samples are calculated under reaction condition at 220 °C in 8 MPa H_2, and specific rates of Re_5/AC-y samples are at 220 °C in 10 MPa H_2, weight ratio of DMCD/catalyst=16:1.

The reducibility and redox behavior of different samples are studied by H_2-TPR (Figure 1C). Two reduction peaks locating at 300-400 °C and 600 °C can be observed in the samples. The reduction peak at lower temperature (denoted as α peak) should be ascribed to the surface or subsurface metal species in oxidization states [24-26], and the peak at higher temperature is assigned to the methanation of carbon with H_2 to form CH_4 [27]. The desorption temperature of α peak varies as a function of Re contents. The α reduction peak in Re_1/AC is maximized

at 390 ^{o}C. Moderate raising of the Re contents (Re_5/AC and Re_7/AC samples) results in the reduction peak towards lower temperature (310 ^{o}C) with much intensified peak heights. The further increase of Re content to 9 wt% leads to slight delay of the α peak to 340 ^{o}C. For better comparison, the reduction peaks have been deconvoluted and the H_2 consumption of the α peak is evaluated as listed in Table 1. Both the intensity and related H_2 consumption of the α peak clearly raises with the metal loading. However, it is worth noting that although the Re loading increments in different Re_x/AC samples, the area of the α peak does not change proportionally. The H_2 consumption by Re_9/AC is only about 2.3-fold higher than the Re_1/AC sample. It is inferred that the metal surface dispersion or even the Re-C interaction might be distinctive by Re decoration in different samples. No matter how, appropriate amount of Re on activated carbon enhances the reducibility of metal precursor, and the rhenium species could be further modulated after the H_2 thermal treatment.

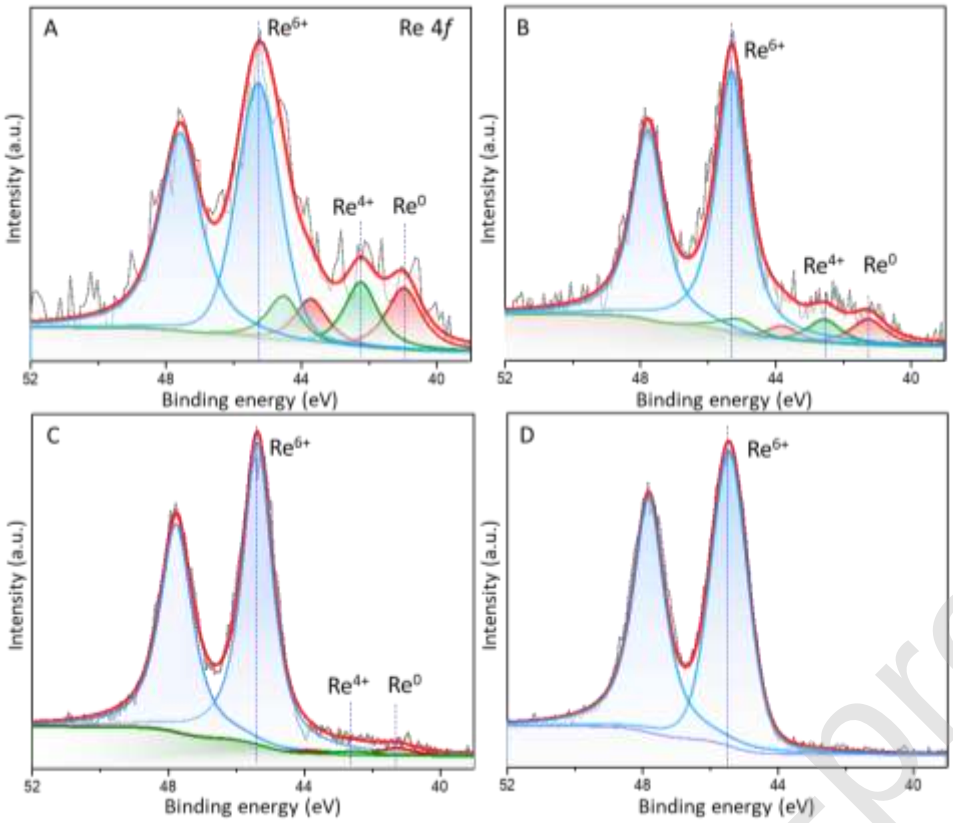

Figure 2. XPS spectra in the Re4*f* region of different reduced samples: Re_3/AC (A), Re_5/AC (B), Re_7/AC (C), and Re_9/AC samples (D).

The detailed information of surface metal composition in the reduced catalyst is further revealed by XPS spectra in the Re4*f* region. The overlapped peaks of rhenium species can be deconvoluted into two sets of peaks due to a doublet Pd $4f_{7/2}$ and $4f_{5/2}$ signals. The binding energy in the Re $4f_{7/2}$ region at about 40.8 eV, 42.4 eV, 45.4 eV should be related to the Re^0, Re^{4+}, and Re^{6+} species [28, 29], respectively. Multiple chemical valences are revealed in different samples with Re^{6+} species as the main composition even after H_2 reduction at 460 °C. In the Re_3/AC sample, 69% Re^{6+} species exists together with small amount of Re^{4+} (16%) and Re^0 (15%), as listed in Table 2. Even lower amounts of Re^{4+} (12%) and Re^0 (12%) species are detected in Re_5/AC. While the Re^{4+} and Re^0 species are barely observed in Re_9/AC. It is suggested by the XPS data that small amount of Re decoration (≤ 5 wt%) facilitates the

generation of Re^{4+} and Re^{0} in the reduced states. The binding energy of Re^{6+} species shifts simultaneously from 45.2 eV of Re_3/AC to 45.4 eV of Re_9/AC. Electron transfer is likely to be happened from Re to C, which should be mainly resulted from the enhanced Re-C interaction with rhenium decoration. The surface molar ratio between Re and C is also given in Table 2. The slightly higher ratio of Re/C, about 1.3-2.0 times compared to the theoretical value is consistent with the well dispersion of metal species on the surfaces of carbon.

Table 2 Surface composition of different Re catalysts based on XPS spectra.

Sample	Surface Re species			Surface Re	Surface oxygenated species			
	Re^{6+}	Re^{4+}	Re^{0}	dispersion	C-O(H)	O-C=O	C=O	O/C%
Re_3/AC	69%	16%	15%	0.042	42%	36%	22%	7.2
Re_5/AC	76%	12%	12%	0.063	40%	28%	32%	8.9
Re_7/AC	97%	1%	2%	0.114	27%	26%	47%	7.8
Re_9/AC	100%	-	-	0.169	20%	24%	56%	9.3
Re_5/AC-HO	93%	3%	4%	0.053	31%	31%	35%	7.2
Re_5/AC-N	100%	-	-	0.090	25%	33%	42%	7.3
Re_5/AC-H	65%	16%	19%	0.039	22%	51%	27%	8.1

3.2 Selective hydrogenation from diester to diol

The as-synthesized Re_x/AC catalysts have been used for the selective hydrogenation of dimethyl 1,4-cyclohexanedicarboxylate (DMCD, i.e. diester) to 1, 4-cyclohexanedimethanol (CHDM, i.e. diol) (Table 3). Pure activated carbon did not perform any activity for the hydrogenation. Diverse by-products have been detected during the reaction by different catalysts as listed in Scheme S1 (Supporting information). The target product-CHDM is transformed preferentially from DMCD to the semi-hydrogenated methyl 4-hydroxymethylcyclohexane carboxylate (MHMCC) and subsequent CHDM. Excessive hydrogenation of CHDM forms the 4-Methyl-1-cyclohexanemethanol (MCHM), and even

small percentages of cyclohexane and its derivatives (product d-f in Scheme S1). Inappropriate hydrogenation of MHMCC could also result in the direct removal of one side hydroxyl group and even $–CH_3$ to form cyclohexanecarboxylic acid (a-c). For clearer comparison, the selectivity of the CHDM and relevant by-products including the MHMCC and MCHM are listed in Table 3. The Re_1/AC sample gives only 41% conversion of DMCD with the semi-hydrogenated MHMCC as the major by-product. The incremental content of Re (from 1% to 5%) leads to the further hydrogenation of both the ester groups in DMCD to give the final diol -CHDM. The DMCD conversion and CHDM selectivity increases steadily with the Re content. 93% conversion of DMCD and 58% CHDM selectivity can be reached using the Re_5/AC catalyst. Excessive Re decoration results in stable DMCD conversion around 95% but further transformation of CHDM into other by-products.

Table 3 Catalytic properties of various Re catalysts in the selective hydrogenation of DMCD.[a]

Entry	Catalyst	P (MPa)	Conv. (%)	Selectivity of typical products (%)[b]		
			DMCD	CHDM	MHMCC	MCHM
1	Re_1/AC	8	41	15	0	41
2	Re_3/AC	8	75	32	3	29
3	Re_5/AC	8	93	58	9	10
4	Re_7/AC	8	91	53	12	12
5	Re_9/AC	8	92	49	6	11
6	Re_5/AC-HO	10	81	23	25	3
7	Re_5/AC-N	10	79	26	25	8
8	Re_5/AC-H	10	15	10	53	1
9	Re_5/AC	10	99	67	1	20

[a] Reaction conditions: reaction under H_2 pressure of 8 MPa or 10 MPa at 220 °C for 10 h, weight ratio of

DMCD/catalyst = 4:1. DMCD: Dimethyl 1, 4-cyclohexanedicarboxylate; MHMCC: methyl 4-hydroxymethylcyclohexane carboxylate; CHDM: 1, 4-cyclohexanedimethanol; MCHM: 4-Methyl-1-cyclohexanemethanol. [b] Other detected by-products and the possible formation pathway is illustrated in Scheme S1.

The influences of reaction conditions have been studied by using Re_5/AC as a typical sample (Figure 3). Both the reaction temperature and pressure affect the distribution of products. Lower temperature causes the direct formation of semi-hydrogenated MHMCC with only one side of ester group transferred into alcohol. The final yield of diol (CHDM) increases volcanically with the reaction temperature and reaches its maximum around 220 ^{o}C. Further raising of temperature leads to the formation of MCHM due to the excessive hydrogenation of one -CH_2OH into -CH_3. The variation of reaction pressure performs similar trend on the distribution of products. Reaction condition under 10 MPa H_2 at 220 ^{o}C gives the better selectivity of diol at 66% with nearly complete conversion of diester. It is visible that MHMCC and CHDM are formed as the initial product within the first 4 h. CHDM is accumulated with the prolonged reaction time, which should be transformed from the MHMCC.

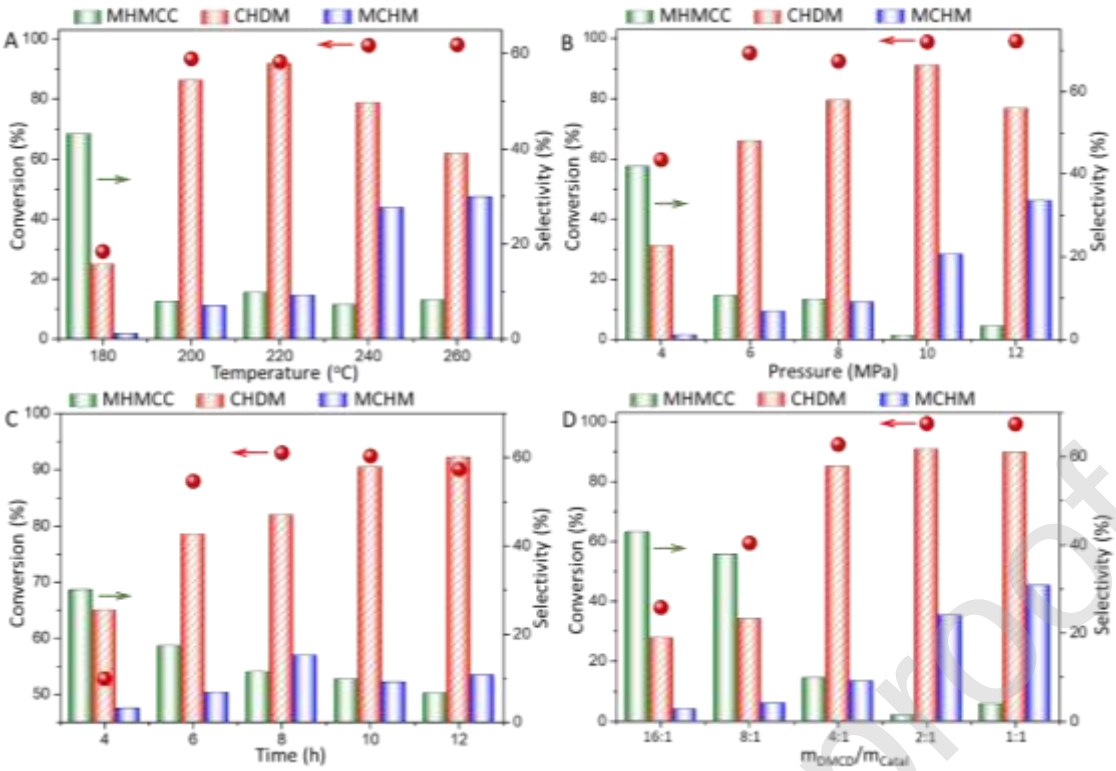

Figure 3. Catalytic performances of Re_5/AC for the selective hydrogenation of dimethyl 1, 4-cyclohexanedicarboxylate (DMCD) as a function of reaction temperature (A), reaction pressure (B), reaction time (C), and catalyst dosage (D). MHMCC: methyl 4-hydroxymethylcyclohexane carboxylate; CHDM: 1, 4-cyclohexanedimethanol; MCHM: 4-Methyl-1-cyclohexanemethanol. Conditions: reaction under H_2 pressure of 8 MPa at 220 °C for 10 h, weight ratio of DMCD/catalyst = 4:1, if not specified.

For better understanding the hydrogenation process, the conversion of DMCD and selectivity of products as a function of the catalyst dosage are shown in Figure 3D. The decrease of catalyst dosage results in the higher amount of semi-hydrogenated MHMCC, due to the insufficient hydrogenation ability by the less amount of catalyst. Whilst excessive dosage of catalyst (weight ratio of reactant/catalyst < 4:1) causes the drastic hydrogenation process to form excessively hydrogenated MCHM with -CH_3. It is interesting that although the higher dosage of catalyst restrains the formation of other complex products, the yield of DMCD could not be further facilitated. In addition, Re species decorated carbon with different pre-treatments have also been synthesized and tested for comparison (Table 2, entry 6-9),

including the H_2 thermal treatment (Re_5/AC-H), H_2O_2 treatment (Re_5/AC-HO), HNO_3 treatment (Re_5/AC-N), and H_2/HNO_3 bi-functionalization (Re_5/AC). It is remarkable that the pre-treatments of activated carbon result in the distinctive catalytic behaviors. The Re_5/AC-H displays only 15% conversion of diester (DMCD) at 220 ^oC for 10 h. However, semi-hydrogenated MHMCC is produced as the main by-product and the selectivity of diol is as low as 10%. An additional by-product (product g in Scheme S1) was also detected occasionally in the reaction solution, mainly caused by the condensation between DMCD and isopropanol, which is only observed by using Re_5/AC-H. The Re_5/AC-HO and Re_5/AC-N samples have nearly identical catalytic performances with 81% and 79% conversion of DMCD. The selectivity of CHDM are 23% and 26% by Re_5/AC-HO and Re_5/AC-N, respectively. It was reported that H_2O_2 aqueous solution and concentrated HNO_3 behaved as available oxidants to oxidize carbon materials and abundant oxygenated groups were easily generated [30, 31]. Based on the bi-functionalization by both H_2 thermal treatment and subsequent HNO_3 oxidation, the Re_5/AC sample largely facilitates the formation of the target diol product (yield of 66%) with complete conversion of DMCD at 220 ^oC in 10 MPa H_2.

3.3 Phase analysis and surface properties of rhenium catalysts

It is until now suspected that two major elements essential for the catalytic performance and selectivity of diol by the series of Re catalysts: i) The rhenium sites with moderate ability to activate, adsorb, or dissociate both the H_2 and reactant molecules; and ii) The possible roles of surface functionalization and oxygenated groups to modulate the surface distribution of rhenium in Re/AC samples. It is straightforward that the surface chemistry of each sample

should be relevant with their catalytic activities. Herein, XRD is performed subsequently to determine the possible particle sizes and crystal phases in different catalysts (Figure 4), in order to rule out other complex surface and structure parameters. Two broad diffraction peaks at 20-30° and 40-50° related to the (002) and (100) crystal faces of amorphous carbon can be observed in all the samples [32, 33]. After the decoration of Ru species, there is no observation of Re-containing species, independent of the Re content or the pretreatment. Considering the relatively high amount of Re species, especially in Re_7/AC and Re_9/AC, no great accumulation or aggregation is formed by Re species. However, the peak intensity of amorphous carbon largely declines with the raising metal loadings, indicating the degree of aromatization and the aromatic planar molecular size were influenced by metal decoration. Re species may change the surface of activated carbon by surface decoration or even inserting, which may split the support into small and randomly oriented sheets [34, 35].

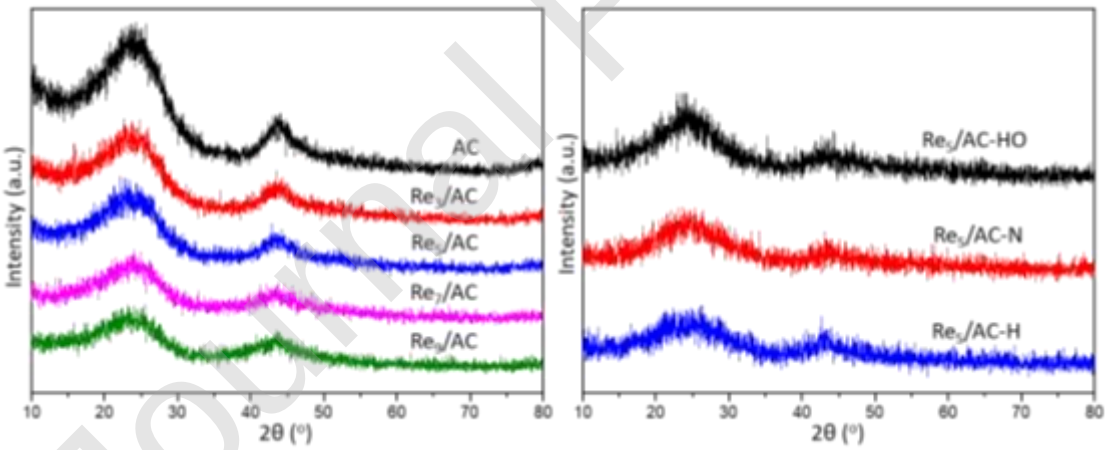

Figure 4. XRD patterns of Re_x/AC-y samples with different Re loadings and pretreatments of activated carbon.

The easy formation of small ReO_x particles not only change the micro-structure of carbon, but may also alter the surface chemical environment of the catalysts. In order to analyze the

surface acidity that may be generated by the carbon surface and the Re decoration, NH_3-TPD are further carried out. One intensive and broad desorption peak appears with its maximum around 600 ^oC (not shown), mainly due to the reaction between C and NH_3 to form one sharp desorption peak. Overlapped desorption peaks can be observed in the range of 100-400 ^oC, as enlarged in Figure 5A-B. Pure carbon support displays two desorption peaks maximized at 110 ^oC and 270 ^oC, corresponding to the weak acid sites and medium strong acid sites [36, 37]. The surface acidity of the activated carbon might be from the surface functionalized oxygenated groups such as –COOH and C-O(H) groups [38, 39]. After Re decoration, the distribution of acid sites largely varies. In general, metal decoration in Re_1/AC leads to the weakening of both the weak and medium strong acid sites. Formation of new acid sites at about 350 ^oC are observed. As the Re content increases, the peak location of the medium strong acid sites shifts from 350 ^oC to 280 ^oC with much intensified peak area. Whilst the desorption temperature of the weak acid sites is not obviously changed, confirming the unchanged type of weak acid sites. The series of Re_5/AC-y samples (Figure 5B) with different pretreatments display nearly identical location and peak area of the desorption peaks, unless the much delayed desorption peak at 300-350 ^oC in Re_5/AC-H. It is also necessary to mention that only Re decorated carbon materials have the methanation peak at about 600 ^oC (Figure S1 in supporting information), whilst activated carbon does not display any observable peak in the range of 400-700 ^oC. Rhenium decoration facilitated the activation of carbon surface. It is also visualized that the surface acidity of rhenium catalysts, or more accurately the medium strong acid sites, is directly correlated with the surface dispersed rhenium species.

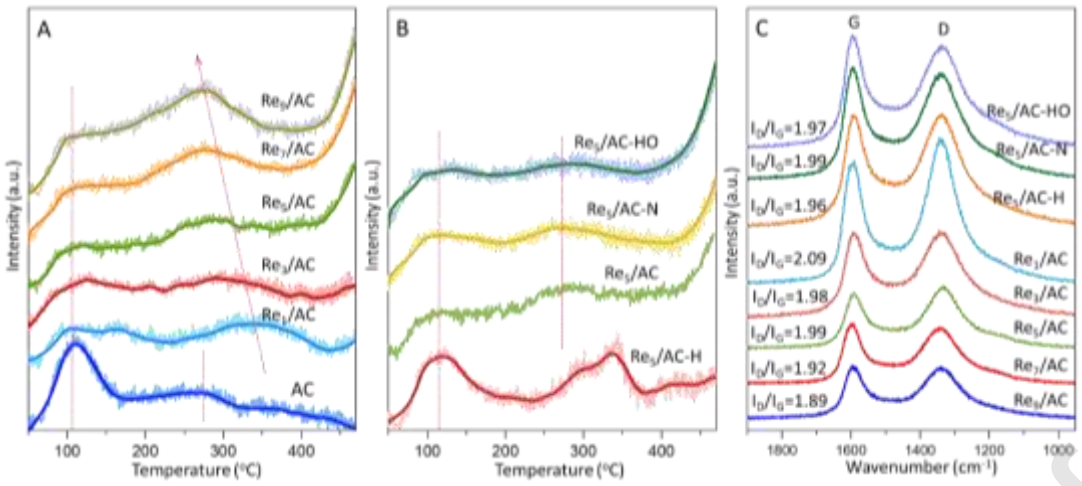

Figure 5. NH_3-TPD profiles (A-B) and Raman spectra (C) of different Re_x/AC-y samples.

In fact, the chemical etching may also happen during pretreatment and Re decoration, resulting in the modified surface micro-structure and can be revealed by the Raman spectra (Figure 5C) [40]. In the wavenumber range of 1800-1000 cm^{-1}, two broad peaks are displayed at 1570 and 1340 cm^{-1}, representing the structural defects and partially disordered structures of the sp^2 domains (D band) and the E_{2g} vibration mode of sp^2 C domains corresponding to the graphitization (G band), respectively. The intensity value of the two peaks (I_D/I_G) suggests the percentage of sp^3 hybridized carbon atoms in the framework of carbon, viewed as a sign of the defect degree. Compared to the I_D/I_G value of the pure activated carbon (1.45), the related value after rhenium decoration is in the range of 1.8-2.1, and the calculated value of defect density is listed in Table 1. It is generally consistent with reports that metal doping or inserting may largely lead to the formation of structure defects [40, 41], which also supports the assumption of XRD results. However, as the Re loading increases, the I_D/I_G decreases from 2.09 to 1.89. It is inferred that rhenium decoration results in changes on the carbon surface, and imperfect surface defects are generated surrounding small ReO_x particles at lower Re content. Whilst excessive ReO_x particles are formed at higher Re content, which may cause

the sinking or blocking of surface instead of regional defects. On the contrary, the defect structure is not greatly influenced by different pretreatment of activated carbon only if the decorated Re content was similar (5 wt%) in this work.

Oxygenated groups may simultaneously generated with surface defects during the synthesis and pretreatment [42, 43]. And the XPS spectra in the O1*s* region is shown in Figure 6. The broad O1*s* peak can be deconvoluted into three overlapped peaks. The peaks at binding energy of 533.5 eV, 532.5 eV and 531.0 eV are corresponding to C-O(H), O-C=O, and C=O of carbon, respectively [41, 44]. The atomic ratio between O/C of different catalysts varies in the range of 7.0%-9.5% (Table 2), slightly raises with the incremental Re loadings. The lattice oxygen in the as-formed ReO_x species also contributes to the distribution of surface oxygen species at 531.5-530.0 eV, overlapping with the C=O species of carbon. It is also remarkable that both the percentages of C-O and O-C=O species obviously decrease along with the Re content. Considering the weakening of acid sites on carbon and the increased value of I_D/I_G after Re decoration, it is rational that ReO_x particles are generated occupying the surface oxygenated groups, especially the C-O and O-C=O groups. The new generated lattice oxygen in ReO_x replenishes the raising percentage of oxygen species at 531.0 eV from 21% to 56% as the Re loading raises from 3% to 9%. The different types of pretreatments also cause the variation of the O/C ratio. Pretreatments of activated carbon by H_2O_2 and HNO_3 lead to similar O/C ratio and distribution of surface oxygen species. Using activated carbon after H_2 thermal treatment, the Re_5/AC-H sample have 51% O-C=O coming from the anhydride and carboxyl groups, which partially accounts for the much intensified desorption peaks in NH_3-TPD of Re_5/AC-H, compare with other samples.

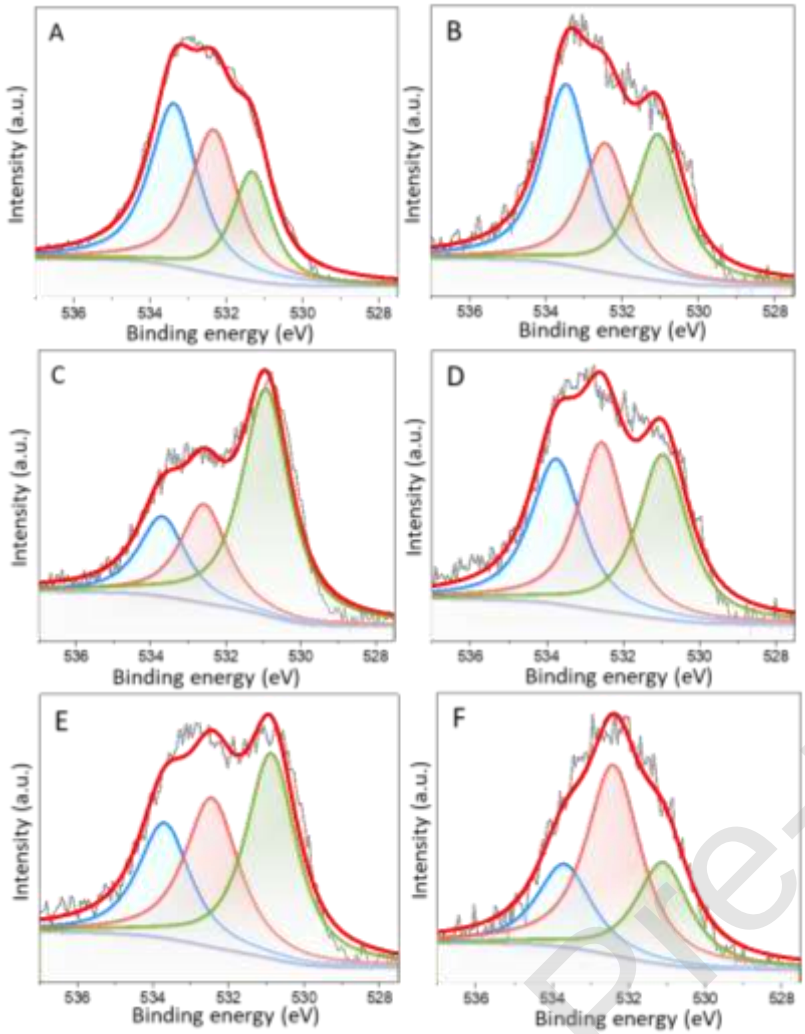

Figure 6. XPS spectra in the O1s region of Re_3/AC (A), Re_5/AC (B), Re_9/AC (C), Re_5/AC-HO (D), Re_5/AC-N (E), and Re_5/AC-H (F) samples.

For better confirmation of the metal surface distribution and other surface information, the STEM and high-resolution TEM of Re_5/AC are illustrated in Figure 7A-B. The shining spots in Figure 7A suggest the surface distribution of ReO_x particles. Small Re particles are formed on the surface of activated carbon. Two different location in the TEM images are amplified as shown in Figure 7B-I and B-II. The high-resolution TEM images illustrate the distribution of ellipsoidal particles on the surface of activated carbon. The interplanar distances of 2.24 Å, 2.09 Å and 1.90 Å are measured and are corresponding to the (002), (201) and (111)

crystal faces of ReO_3. The intersection angle of 65° and 53° between different crystal faces in Figure 7B-I further confirms the existence of ReO_3 phases. Very small and spherical ReO_3 particles about 2 nm are also observed on the surface of activated carbon, as pointed by the dotted cycle in Figure 7B-II. It is inferred that small ReO_3 particles are readily formed in the Re_5/AC sample and are possibly melted to form the ellipsoidal particles, due to the surface orientation effect during thermal treatment. The ReO_3 (111) crystal faces are more frequently exposed with extensive surface platform in the special ellipsoidal particles. Interestingly, terrace sites are likely to be generated and exposed due to the interlaced (111) and (002) crystal faces as shown by the arrows in Figure 7B-I.

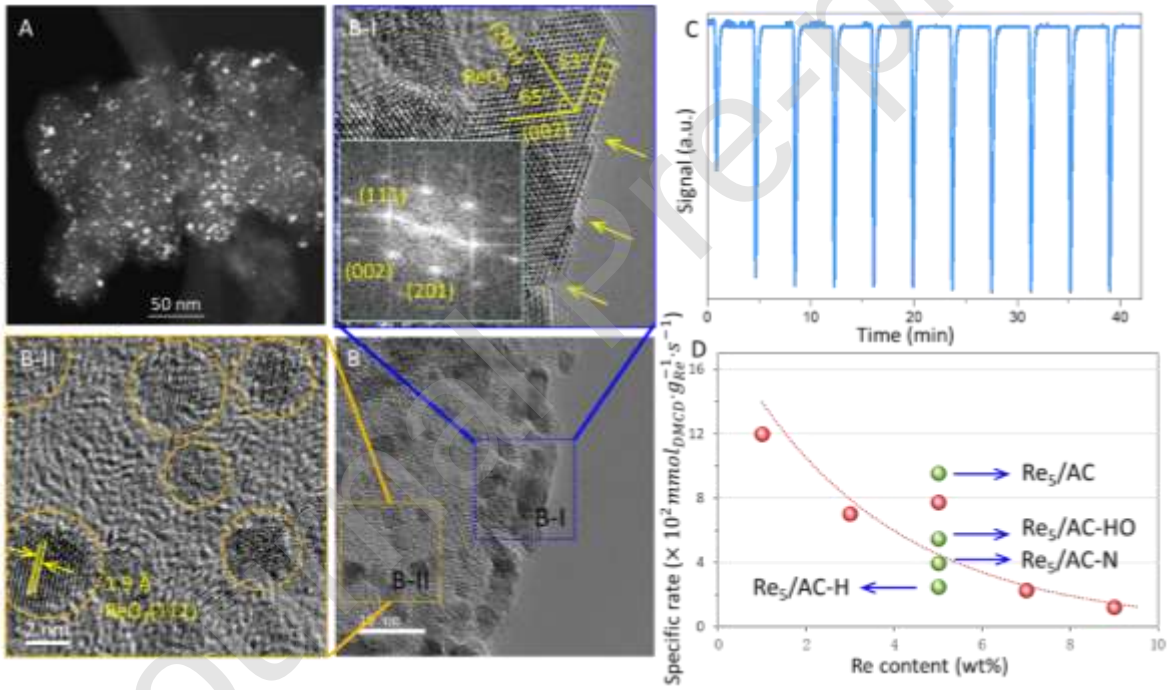

Figure 7. STEM image (A), high-resolution TEM images (B), and CO chemisorption by pulse (C) of typical Re_5/AC sample, and the relationship between specific rate and Re content (D), B-I and B-II are the enlarged parts in the dotted box of B. The arrows in B-I point out the terrace sites of ReO_3 composition. And the dotted cycles in B-II illustrate the well-formed small particles around 2 nm. The red balls in D show the specific rates of Re_x/AC at 220 °C in 8 MPa H_2, and green balls suggest the specific rates of different Re_5/AC-y samples at 220 °C in 10 MPa H_2.

No matter how, the stability of the monometallic Re/AC still has to be enhanced. The

catalytic performance of the Re_5/AC sample is not satisfied as the DMCD conversion decreases continuously during the four-time reaction cycles (Figure S2). The selectivity of CHDM also decreases during the third time of reaction. It is suggested that the re-used sample becomes incompetent to activate the diester and to hydrogenate the intermediate in depth, mainly due to the variation of its surface composition or the structure. The TEM image of used Re_5/AC sample is displayed in Figure S3. It is observable that particles on the surface of AC seem to be surrounded by the rough surface of amorphous carbon, which is possibly formed during the reaction and causes the coking on the catalyst. The failed exposure of the active ReO_x species is responsible for the much watered-down catalytic behavior. Promoted Re/AC catalyst with availably and stably exposed ReO_x sites should be more reliable for the reaction.

3.4 On the acting roles of rhenium decoration

Until now, it is generally clear that Re decoration on activated carbon is responsible for not only the active metal sites, but also for the great modifications on both the surface chemical environment and micro-structure. Combining the results from XPS and NH_3-TPD, the decoration of Re is mostly accomplished by the rhenium species occupying the surface oxygenated groups on carbon during surface functionalization. The new generated ReO_x species changes the porous structure and the surface defect density of carbon. The specific rates according to the exposed Re active sites are evaluated based on the CO chemisorption as listed in Table 1 and Figure 7C-D. Unlike the exponentially increased CHDM yield, the specific rate of Re_x/AC samples losses as a function of the Re content. The Re_1/AC sample displays the much exaggerated specific rate of $11.9 \times 10^2\ mmol_{DMCD} \cdot g_{Re}^{-1} \cdot h^{-1}$, indicating

its superior utilization of each exposed metal atom compared to the other samples with higher Re contents. The specific rates of Re_5/AC are calculated to be 7.7×10^2 and $9.5 \times 10^2\ mmol_{DMCD} \cdot g_{Re}^{-1} \cdot h^{-1}$, under 8 MPa and 10 MPa H_2 at 220 °C, respectively. It has to be noted that only Cr based catalysts have been reported on an industrial scale. Thus the current result based on Re catalyst has been compared with the reported literature (Table S1). Although Cu based catalysts displayed higher CHDM yield compared to the current and reported work based on precious metals, the Cu loadings were extremely high [45, 46]. The calculated specific rate of the reported Cu/ZnO/ZrO_2 catalyst was only 16.8 mmol/g_{Cu}/h at 220 °C in 8 MPa H_2 [47]. Other bimetallic Ru-Sn samples and even trimetallic samples were reported for the selective hydrogenation process to give CHDM [48, 49]. However, higher reaction temperature and excessive use of precious metals were necessary for better activity. No matter how, Re based catalyst can be potentially applied to the selective production of CHDM with further constructive modification.

As a direct result of the lower Re content, finer ReO_x particles with Re species in reduced states (Re^0 and Re^{4+}) are also facilitated to be dispersed on the surface only if the Re loading was lowered to 5 wt% and even less. Such phenomenon suggests that the selective hydrogenation of DMCD might be structure-sensitive. No matter how, although the ReO_x particles slightly accumulate due to the shortened distances between neighboring particles, there is no sign of great sintering at high Re loading as revealed by XRD and TEM. Herein, it is more rational to propose the surface dispersion of exposed active Re sites (Table 1), instead of the ReO_x particle sizes, that are adjusted controllably by the Re decoration content. Appropriately enhanced Re content is preferential to produce selectively the target CHDM

with enough power. The higher surface dispersion of ReO_x inducing the better redox property of the catalyst and the more observable interaction between Re and carbon. Electron transformation has been confirmed from Re species to the neighboring C atoms to give the availably exposed electron-deficient Re sites. In the typical Re_5/AC sample, ellipsoidal particles exist with terrace sites at the cross interfaces of (111) and (002) faces. Large amount of medium strong acid sites are constructed simultaneously, which positively accelerate relevant with the catalytic performance.

4. Conclusion

A series of Re catalysts on activated carbon have been synthesized and used for the selective hydrogenation of diester to diol. The initial influences on both the Re surface dispersion and pretreatment of activated carbon have been investigated. ReO_x particles were readily generated by occupying the surface oxygenated groups on carbon (mostly C-O(H) and (H)O-C=O groups). Fine ReO_x particles were dispersed on the carbon surface independent of the synthesis conditions, mainly due to the initial electron-positive property and its electron transferred from Re to C. It ascribed subsequently for the much facilitated reducibility of the catalyst and the maintenance of Re^{6+} even after H_2 reduction. ReO_x species as electron acceptor could further act as appropriate acid sites and adsorb the reactant more readily. Re species in the reduced states could still be maintained under appropriate Re surface dispersion. The moderate hydrogenation ability of Re based catalyst restrained the excessive hydrogenation of CHDM to other by-products. The complete conversion of diester and 66% yield of diol can be reached with the specific rate of $9.5 \times 10^2\ mmol_{DMCD} \cdot g_{Re}^{-1} \cdot h^{-1}$ at 220

^{o}C under 10 MPa H_2.

Author Statement

Jingjie Luo: Conceptualization, Investigation, Writing - Original Draft. **Enhui Qu**: Data curation, Investigation. **Yixue Zhou**: Validation, ***Yanan Dong:*** Formal analysis. **Changhai Liang**: Writing- Reviewing and Editing, Supervision, Project administration, Funding acquisition,

Declaration of interests

The authors declare that they have no known competing financial interests or personal relationships that could have appeared to influence the work reported in this paper.

Acknowledgements

This work was supported by the National Natural Science Foundation of China (21573031, 21978031 & 21802015), and Program for Excellent Talents in Dalian City (2016RD09, 2016RD04). The authors acknowledge Dr. Zhanglong Guo for the experimental assistance of STEM and HRTEM.

References

[1] J. Wang, S. Mahmud, X. Zhang, J. Zhu, Z. Shen, X. Liu, Biobased amorphous polyesters with high T_g: Trade-off between rigid and flexible cyclic diols. Acs Sustain. Chem. Eng. 7 (2019) 6401-6411. https://doi.org/10.1021/acssuschemeng.9b00285.

[2] S. Hahm, J.-S. Kim, H. Yun, J.H. Park, R.A. Letteri, B.J. Kim, Bench-scale synthesis and

characterization of biodegradable aliphatic–aromatic random copolymers with 1,4-cyclohexanedimethanol units toward sustainable packaging applications. Acs Sustain. Chem. Eng. 7 (2019) 4734-4743. https://doi.org/10.1021/acssuschemeng.8b04720.

[3] M. Matos, A.F. Sousa, A.J.D. Silvestre, Improving the thermal properties of poly(2,5-furandicarboxylate)s using cyclohexylene moieties: A comparative study. Macromol. Chem. Phys. 218 (2017) 1600492. https://doi.org/10.1002/macp.201600492.

[4] A. Guarneri, V. Cutifani, M. Cespugli, A. Pellis, R. Vassallo, F. Asaro, C. Ebert, L. Gardossi, Functionalization of enzymatically synthesized rigid poly(itaconate)s via post-polymerization Aza-Michael addition of primary amines. Adv. Synth. Catal. 361 (2019) 2559-2573. https://doi.org/10.1002/adsc.201900055.

[5] G. Lewandowski, A. Wroblewska, E. Milchert, Synthesis of 1,4-cyclohexanedimethanol by hydrogenation of dimethyl terephthalate and its application as a substrate in syntheses of polyesters. Polimery-W 52 (2007) 39-43. https://doi.org/10.14314/polimery.2007.039.

[6] S.Y. Zhang, Q. Hu, G.L. Fan, F. Li, The relationship between the structure and catalytic performance Cu/ZnO/ZrO_2 catalysts for hydrogenation of dimethyl 1,4-cyclohexane dicarboxylate. Catal. Commun. 39 (2013) 96-101. http://doi.org/10.1016/j.catcom.2013.05.011.

[7] J.M. Thomas, B.F.G. Johnson, R. Raja, G. Sankar, P.A. Midgley, High-performance nanocatalysts for single-step hydrogenations. Accounts Chem. Res. 36 (2003) 20-30. http://doi.org/ 10.1002/ chin.200316294.

[8] R. Raja, T. Khimyak, J.M. Thomas, S. Hermans, B.F.G. Johnson, Single-step, highly active, and highly selective nanoparticle catalysts for the hydrogenation of key organic compounds. Angew. Chem. Int. Edit. 240 (2001) 4638-4642. https://doi.org/10.1002/1521-3773(20011217)40:24<4638::AID-ANIE4638>3.0.CO;2-W.

[9] Q. Hu, G.L. Fan, S.Y. Zhang, L. Yang, F. Li, Gas phase hydrogenation of dimethyl-1,4-cyclohexane dicarboxylate over highly dispersed and stable supported copper-based catalysts. J. Mol. Catal. a-Chem. 397 (2015) 134-141. http://doi.org/10.1016/j.molcata.2014.10.032.

[10]J. Zhang, C. Li, X. Chen, Y. Chen, L. Zhang, B. Zhang, C. Liang, Promotional effects of magnesia on catalytic performance of Pt/SiO_2 in hydrogenolysis of dibenzofuran. J. Catal. 371 (2019) 346-356. https://doi.org/10.1016/j.jcat.2019.02.017.

[11]J.M. Keels, X. Chen, S. Karakalos, C. Liang, J.R. Monnier, J.R. Regalbuto, Aqueous-phase hydrogenation of succinic acid using bimetallic Ir–Re/C catalysts prepared by strong electrostatic adsorption. Acs Catal. 8 (2018) 6486-6494. https://doi.org/10.1021/acscatal.8b01006.

[12]X.X. Dong, B.S. Jin, Y.Q. Sun, L. Yu, Urban gas production from low H_2/CO biogas using Re-promoted Ni catalysts supported on modified manganese sand. Fuel 220 (2018) 60-71. http://doi.org/10.1016/j.fuel.2018.01.128.

[13]X. Jin, P.S. Thapa, B. Subramaniam, R.V. Chaudhari, Kinetic modeling of sorbitol hydrogenolysis over bimetallic RuRe/C Catalyst. Acs Sustain. Chem. Eng. 4 (2016) 6037-6047. http://doi.org/10.1021/acssuschemeng.6b01346.

[14]T. Ayvali, P.F. Fazzini, P. Lecante, A. Mayoral, K. Philippot, B. Chaudret, Control of reactivity through chemical order in very small RuRe nanoparticles. Dalton T. 46 (2017) 15070-15079. http://doi.org/10.1039/C7DT02287E.

[15]X. Di, C. Li, B.S. Zhang, J. Qi, W.Z. Li, D.S. Su, C.H. Liang, Role of Re and Ru in Re-Ru/C bimetallic catalysts for the aqueous hydrogenation of succinic acid. Ind. Eng. Chem. Res. 56 (2017) 4672-4683. http://doi.org/10.1021/acs.iecr.6b04875.

[16]X. Di, C. Li, G. Lafaye, C. Especel, F. Epron, C.H. Liang, Influence of Re-M interactions in Re-M/C bimetallic catalysts prepared by a microwave-assisted thermolytic method on aqueous-phase hydrogenation of succinic acid. Catal. Sci. Technol. 7 (2017) 5212-5223. http://dio.org/10.1039/c7cy01039g.

[17]Z.-Y. Li, M.S. Akhtar, D.-H. Kwak, O.B. Yang, Improvement in the surface properties of activated carbon via steam pretreatment for high performance supercapacitors, Appl. Surf. Sci. 404 (2017) 88-93. https://doi.org/10.1016/j.apsusc.2017.01.238.

[18]L.G. Cançado, A. Jorio, E.H.M. Ferreira, F. Stavale, C.A. Achete, R.B. Capaz, M.V.O. Moutinho, A. Lombardo, T.S. Kulmala, A.C. Ferrari, Quantifying defects in graphene via Raman spectroscopy at different excitation energies, Nano Lett. 11(8) (2011) 3190-3196. https://doi.org/10.1021/nl201432g.

[19]E.H. Martins Ferreira, M.V.O. Moutinho, F. Stavale, M.M. Lucchese, R.B. Capaz, C.A. Achete, A. Jorio, Evolution of the Raman spectra from single-, few-, and many-layer graphene with increasing disorder, Phys. Rev. B 82(12) (2010) 125429. https://doi.org/10.1103/PhysRevB.82.125429.

[20]J.L. Fan, J. Xiao, D.Y. Liu, G.P. Ye, J.F. Luo, D. Houlbrooke, S. Laurenson, J. Yan, L.J. Chen, J.P. Tian, W.X. Ding, Effect of application of dairy manure, effluent and inorganic fertilizer on nitrogen leaching in clayey fluvo-aquic soil: A lysimeter study. Sci. Total. Environ. 592 (2017) 206-214. http://doi.org/10.1016/j.scitotenv.2017.03.060.

[21]P. Zhang, J. Zhang, S. Dai, Mesoporous carbon materials with functional compositions. Chem.-Eur. J. 23 (2017) 1986-1998. https://doi.org/10.1002/chem.201602199.

[22]J. Wang, Q. Liu, An ordered mesoporous aluminosilicate oxynitride template to prepare N-incorporated ordered mesoporous carbon. J. Phys. Chem. C 111 (2007) 7266-7272. https://doi.org/10.1021/jp070187h.

[23]P. Peng, D. Stosic, X.M. Liu, Z.F. Yan, S. Mintova, Strategy towards enhanced performance of zeolite catalysts: Raising effective diffusion coefficient versus reducing diffusion length, Chem. Eng. J. 385 (2020) 123800. http://doi.org/10.1016/j.cej.2019.123800.

[24]W. Cao, L. Lin, H. Qi, Q. He, Z. Wu, A. Wang, W. Luo, T. Zhang, In-situ synthesis of single-atom Ir by utilizing metal-organic frameworks: An acid-resistant catalyst for hydrogenation of levulinic acid to γ-valerolactone. J. Catal. 373 (2019) 161-172. https://doi.org/10.1016/j.jcat.2019.03.035.

[25]N. Ota, M. Tamura, Y. Nakagawa, K. Okumura, K. Tomishige, Performance, structure, and mechanism of ReO_x-Pd/CeO_2 catalyst for simultaneous removal of vicinal OH groups with H_2. Acs Catal. 6 (2016) 3213-3226. http://doi.org/10.1021/acscatal.6b00491.

[26] S.Y. Xu, F.Q. Xie, H.M. Xie, G.L. Zhou, X.Y. Liu, Effect of structure and composition on the CO_2 hydrogenation properties over bimodal mesoporous CeCo composite catalyst, Chem. Eng. J. 375 (2019) 122023. http://doi.org/10.1016/j.cej.2019.122023.

[27] E.H. Qu, J.J. Luo, X. Di, C. Li, C.H. Liang, Selective hydrogenation of dimethyl terephthalate to 1,4-cyclohexane dicarboxylate by highly dispersed bimetallic Ru-Re/AC catalysts. J. Nanosci. Nanotechno. 20 (2020) 1140-1147. http://doi.org/10.1016/j.molcata.2014.10.032.

[28] K. Baranowska, J. Okal, Bimetallic Ru-Re/γ-Al_2O_3 catalysts for the catalytic combustion of propane: Effect of the Re addition, Appl. Catal. a-Gen. 499 (2015) 158-167. http://doi.org/j.apcata.2015.04.023.

[29] J. Okal, XPS study of oxidation of rhenium metal on γ-Al_2O_3 support, J. Catal. 225 (2004) 498-509. http://doi.org/j.jcat.2004.05.004.

[30] J.J. Luo, Y.F. Liu, H. Wei, B.L. Wang, K.H. Wu, B.S. Zhang, D.S. Su, A green and economical vapor-assisted ozone treatment process for surface functionalization of carbon nanotubes. Green Chem. 19 (2017) 1052-1062. http://doi.org/10.1039/C6GC02806C.

[31] F.X. Xiao, G.H. Jiao, H. Shen, K.B. Li, Y.Z. Ouyang, W.Z. Zhang, G.B. Chen, Y. Peng, Influences of pretreatment of carbon on performance of carbon supported Pd nanocatalyst for nitrobenzene hydrogenation, J. Nanosci. Nanotechno. 20 (2020) 629-635. http://doi.org/10.1166/jnn.2020.16882.

[32] S. Hu, K.J. Xie, X.M. Zhang, S.P. Zhang, J.J. Gao, H.O. Song, D.Z. Chen, Significantly enhanced capacitance deionization performance by coupling activated carbon with triethyltetramine-functionalized graphene. Chem. Eng. J. 384 (2020) 123317. http://doi.org/10.1016/j.cej.2019.123317.

[33] Y.F. Li, X.L. Yan, X.Y. Hu, R. Feng, M. Zhou, Trace pyrolyzed ZIF-67 loaded activated carbon pellets for enhanced adsorption and catalytic degradation of Rhodamine B in water. Chem. Eng. J. 375 (2019) 122003. http://doi.org/10.1016/j.cej.2019.122003.

[34]M.W. Smith, I. Dallmeyer, T.J. Johnson, C.S. Brauer, J.S. McEwen, J.F. Espinal, M. Garcia-Perez, Structural analysis of char by Raman spectroscopy: Improving band assignments through computational calculations from first principles. Carbon 100 (2016) 678-692. http://doi.org/10.1016/j.carbon.2016.01.031.

[35]J. Yang, S. Ren, T. Zhang, Z. Su, H. Long, M. Kong, L. Yao, Iron doped effects on active sites formation over activated carbon supported Mn-Ce oxide catalysts for low-temperature SCR of NO. Chem. Eng. J. 379 (2020) 122398. https://doi.org/10.1016/j.cej.2019.122398.

[36]G.H. Han, M.W. Lee, S. Park, H.J. Kim, J.P. Ahn, M.G. Seo, K.Y. Lee, Revealing the factors determining the selectivity of guaiacol HDO reaction pathways using ZrP-supported Co and Ni catalysts, J. Catal. 377 (2019) 343-357. http://doi.org/10.1016/j.jcat.2019.07.034.

[37]C. Zhang, J. Luo, Y. Zhou, Q. Jiang, C. Liang, Metal oxide sub-nanoclusters decorated Ni catalyst for selective hydrogenation of adiponitrile to hexamethylenediamine, J. Catal. 381 (2020) 14-25. http://doi.org/10.1016/j.jcat.2019.10.024.

[38]J.K. Xie, Q.N. Han, J. Wang, L.J. Bai, J.F. Lu, Z.G. Liu, Enhanced alpha-terpineol yield from alpha-pinene hydration via synergistic catalysis using carbonaceous solid acid catalysts. Ind. Eng. Chem. Res. 58 (2019) 22202-22211. http://doi.org/10.1021/acs.iecr.9b04848.

[39]W.H. Li, Y. Liu, M.C. Mu, F.S. Ding, Z.M. Liu, X.W. Guo, C.S. Song, Organic acid-assisted preparation of highly dispersed Co/ZrO_2 catalysts with superior activity for CO_2 methanation. Appl. Catal. B-Environ. 254 (2019) 531-540. http://doi.org/10.1016/j.apcatb.2019.05.028.

[40]H. Yuan, D. Guo, X. Li, L. Yuan, W. Zhu, L. Chen, X. Qiu, The effect of CeO_2 on Pt/CeO_2/CNT catalyst for CO electrooxidation. Fuel Cells 9 (2009) 121-127. http://doi.org/10.1002/fuce.200800100.

[41]Y. Dong, J. Luo, S. Li, C. Liang, CeO_2 decorated Au/CNT catalyst with constructed Au-CeO_2 interfaces for benzyl alcohol oxidation. Catal. Commun. 133 (2020) 105843. https://doi.org/10.1016/j.catcom.2019.105843.

[42] S. Yuan, T. Li, Y. Wang, B. Cai, X. Wen, S. Shen, X. Peng, Y. Li, Double-adsorption functional carbon based solid acids derived from copyrolysis of PVC and PE for cellulose hydrolysis. Fuel 237 (2019) 895-902. https://doi.org/10.1016/j.fuel.2018.10.088.

[43] Y. Lin, Y. Li, Z. Xu, J. Xiong, T. Zhu, Transformation of functional groups in the reduction of NO with NH_3 over nitrogen-enriched activated carbons. Fuel 223 (2018) 312-323. https://doi.org/10.1016/j.fuel.2018.01.092.

[44] J.J. Luo, H. Wei, Y.F. Liu, D. Zhang, B.S. Zhang, W. Chu, C. Pham-Huu, D.S. Su, Oxygenated group and structural defect enriched carbon nanotubes for immobilizing gold nanoparticles. Chem. Commun. 53 (2017) 12750-12753. http://doi.org/10.1039/c7cc06594a.

[45] H. Liu, Q. Hu, G. Fan, L. Yang, F. Li, Surface synergistic effect in well-dispersed Cu/MgO catalysts for highly efficient vapor-phase hydrogenation of carbonyl compounds, Catal. Sci. Technol. 5(8) (2015) 3960-3969. https://doi.org/10.1039/C5CY00437C.

[46] S. Zhang, G. Fan, F. Li, Lewis-base-promoted copper-based catalyst for highly efficient hydrogenation of dimethyl 1,4-cyclohexane dicarboxylate, Green Chem. 15(9) (2013) 2389-2393. https://doi.org/10.1039/C3GC40658J.

[47] S. Zhang, Q. Hu, G. Fan, F. Li, The relationship between the structure and catalytic performance Cu/ZnO/ZrO_2 catalysts for hydrogenation of dimethyl 1,4-cyclohexane dicarboxylate, Catal. Commun. 39 (2013) 96-101. https://doi.org/10.1016/j.catcom.2013.05.011.

[48] K. Tahara, H. Tsuji, H. Kimura, T. Okazaki, Y. Itoi, S. Nishiyama, S. Tsuruya, M. Masai, Liquid-phase hydrogenation of dicarboxylates catalyzed by supported Ru-Sn catalysts, Catal. Today 28(3) (1996) 267-272. https://doi.org/10.1016/0920-5861(95)00247-2.

[49] X. Li, Z. Sun, J. Chen, Y. Zhu, F. Zhang, One-pot conversion of dimethyl terephthalate into 1,4-cyclohexanedimethanol with supported trimetallic RuPtSn catalysts, Ind. Eng. Chem. Res. 53(2) (2014) 619-625. https://doi.org/10.1021/ie402987c.